ChemComm

Accepted Manuscript

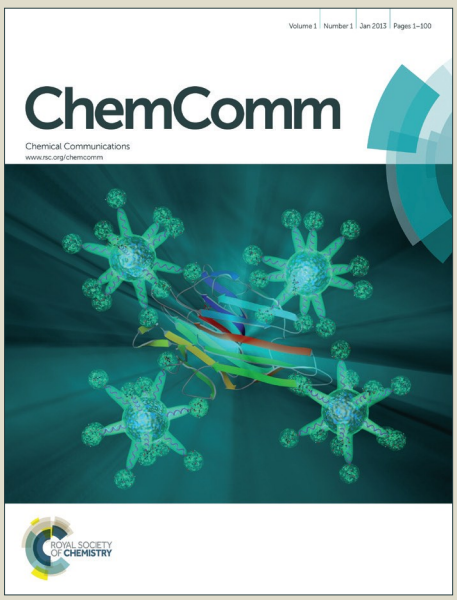

ROYAL SOCIETY OF CHEMISTRY

www.rsc.org/chemcomm

Journal Name

COMMUNICATION

Fluorogenic Nanoreactor Assembly with Boosted Sensing Kinetics for Timely Imaging of Cellular Hydrogen Peroxide

Received 00th January 20xx,
Accepted 00th January 20xx

DOI: 10.1039/x0xx00000x

www.rsc.org/

Jeongyun Heo[a,b,‡], Chang-Keun Lim[a,‡], Youngsun Kim[a], Hong-Jun Cho[a], Yong-Deok Lee[a,c], Joon-ho Maeng[a], Dae-Ro Ahn[a], Sangyoup Lee[a], Joona Bang[c], Soo Young Park[b,*], and Sehoon Kim[a,*]

Precise detection of endogenous H_2O_2 has been considered to be a useful tool for understanding cell physiology. Here, we develop a nanoreactors co-incorporated with a H_2O_2-responsive fluorogenic molecule and a catalytic additive. The fast sensing kinetics allows us to visualize a subcellular response in real-time.

Hydrogen peroxide (H_2O_2) is a mediator molecule that plays crucial roles in various cellular signal transductions related to physiological processes[1-3] as well as pathological effects.[4] It has been found that H_2O_2 is a major reactive oxygen species (ROS) implicated in redox signaling during proliferation and apoptosis of cells[3,5] owing to its relatively high stability.[2,3,6] In cell signaling, stimulation by cellular receptors or enzymes produces H_2O_2 whose concentration and location rely strongly on types of the process of interest. For example, the endogenous concentration of H_2O_2 varies from 10^{-8}-10^{-7} M in proliferation to 10^{-4} M in apoptosis.[2,7] Due to the process-dependent nature of H_2O_2 production, highly resolved imaging of cellular H_2O_2 distribution in both spatial and temporal ways is essential to provide key information in understanding localized subcellular events.[8,9]

Imaging H_2O_2 in living cells by a fluorescence dequenching response of quenched molecular probes has been extensively exploited. Dichlorodihydrofluorescein (DCFH) and its diacetate derivative (DCFH-DA) have been widely used,[10] and other candidate molecules whose fluorescence is quenched by chemical caging with H_2O_2-cleavable moieties such as boronate[11-13] and sulfonate[14-15] were reported for the endogenous detection of H_2O_2. Since fluorogenic H_2O_2 sensing works on a reaction basis, sensitivity is significantly affected by the reaction rate of probe molecules. In this regard, single-molecule probe systems would have critical limits in increasing the reaction rate by modifying the chemical structure, offering generally low sensing rates. There have been reports on real-time imaging of intracellular H_2O_2 with inorganic nanoprobes with switchable photoluminescence.[16] However, it is hard to achieve exact visualization of the spatiotemporal evolution of low-level H_2O_2 at the very beginning of a subcellular event by single-molecule probes without any improvement in reversibility and/or kinetics.

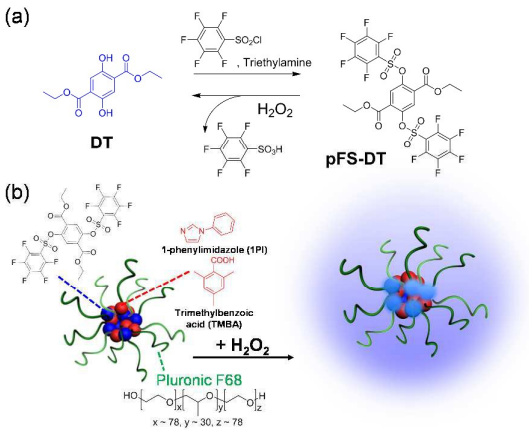

Scheme 1. (a) Synthesis of a fluorescence-quenched probe molecule (pFS-DT) and its reverse (fluorescence dequenching) reaction in response to H_2O_2. (b) Schematic illustration of an all-in-one nanoreactor co-incorporating pFS-DT and catalysts (hydrophobic base or acid) and its H_2O_2–triggered fluorogenic reaction.

Taking reaction kinetics into consideration, we devised a simple way of catalyzing the sensing reaction by integrating molecular probe reactants with catalysts in a nanoreactor. Here, we report a reactor-like fluorogenic nanoprobe in which quenched fluorescent dyes and catalytic additives are densely co-incorporated, enabling imaging of H_2O_2 with improved spatiotemporal resolution during cellular processes. Even though the flurogenic molecule in our nanoreactor has

[a] Center for Theragnosis, Korea Institute of Science and Technology (KIST), 39-1 Hawolgok-dong, Seongbuk-gu, Seoul 136-791, Korea.
[b] Department of Material Science and Engineering, Seoul National University, 599 Gwanak-ro, Gwanak-gu, Seoul 151-744, Korea.
[c] Department of Chemical and Biological Engineering, Korea University, 145 Anam-ro, Seongbuk-gu, Seoul 136-713, Korea.
‡ These authors equally contributed to this work.
Electronic Supplementary Information (ESI) available: experimental details and additional data. See DOI: 10.1039/x0xx00000x

irreversible character, we could achieve the real-time imaging of H_2O_2 at the beginning of the cellular event due to the fast sensing kinetics of our nanoreactor.

Diethyl 2,5-dihydroxyterephthalate (DT) was chosen as a fluorescent unit due to its high fluorescence efficiency (FLQY = 0.71 in THF and 0.45 in water suspension of nanoaggregates) even in the solid state, being suitable for constructing dye-concentrated nanoprobes. Fluorescence of the parent dye (DT) was quenched with the pentafluorophenylsulfonyl (pFS) group[13-14] by bis-sulfonylation of DT led to significant fluorescence quenching (FLQY of pFS-DT = 0.001 in THF solution) with a large hypsochromic shift of the absorption maximum ($\lambda_{max.abs}$) from 380 to 275 nm shown Fig 1(a).

Fluorescence recovery of pFS-DT in response to H_2O_2 was evaluated with different catalytic additives in THF solution. pFS-DT by itself exhibited a fluorogenic response to H_2O_2. The degree of dequenching was enormously enhanced in the presence of a base, triethylamine (TEA), whereas acetic acid (AcOH) showed a retarding effect by which the recovered fluorescence at a given time was weaker than that of pFS-DT itself (Fig 1b). The base-catalyzed enhanced response is attributable to the deprotonation of H_2O_2 into perhydroxide (HOO^-) with enhanced nucleophilicity for perhydrolysis. To understand the origin of the fluorogenic response of pFS-DT, the spectral characteristics were examined with model compounds (Fig S1 and S2 in the Supporting Information). Because pFS-DT is a bis-sulfonylated compound, mono- or di-pFS deprotection is anticipated to occur by H_2O_2–induced perhydrolysis. Model compounds for mono- and di-pFS deprotection manifested distinct absorption, emission, and excitation maxima ($\lambda_{max.abs}$ = 325 nm, $\lambda_{max.em}$ = 380, 468 nm, $\lambda_{max.ex}$ = 325 nm for mono-deprotection; $\lambda_{max.abs}$ = 378 nm, $\lambda_{max.em}$ = 450 nm, $\lambda_{max.ex}$ = 380 nm for di-deprotection). Spectral features of the latter di-deprotected compound (DT) coincide well with those of the H_2O_2–reaction product of pFS-DT, suggesting that DT is the emissive product of the fluorogenic reaction. Gas chromatography/mass spectrometry (GC/MS) confirmed that pFS-DT indeed decomposes into di-deprotected DT in the presence of H_2O_2 and TEA (Fig S3). To nanoscopically confine the above-demonstrated sensing reaction, H_2O_2 nanoreactor probes (NPs) were briefly formulated through homogeneous mixing of catalytic additive and pFS-DT at a given weight ratio with Pluronic F-68 that is a neutral polymeric surfactant forming stable micelles. To introduce base catalysis to the sensing kinetics, 1-phenylimidazole (1PI) was chosen as a hydrophobic base that mimics histidine (His), a key residue of horseradish peroxidase (HRP)[17] involved in H_2O_2 activation. For decelerating the sensing reaction, trimethylbenzoic acid (TMBA) was employed as an acidic decatalyst that would hinder the H_2O_2 deprotonation and thus retard the pFS-DT perhydrolysis. The physically assembled NPs formed a stable aqueous suspension. Base NPs (1PI:pFS-DT=10:1) presented the average diameter and the intensity-weighted hydrodynamic size of 77 ± 17 nm (TEM) and 103 ± 13 nm (DLS), respectively (Fig 1c).

H_2O_2 sensing kinetics of NPs was analyzed with time after addition of 100 μM H_2O_2. The fluorogenic responses with different loading amounts and types of catalytic additives could be expressed by two different kinetic equations (Fig S4a-b). NPs that are uncatalyzed (pFS-DT alone), acid-decatalyzed (TMBA:pFS-DT=10:1) and catalyzed with relatively small amounts of base (1PI:pFS-DT=1:1 and 0.1:1) presented a single-phase fluorescence rise during the whole period of observation. In contrast, NPs catalyzed with excess base (1PI:pFS-DT=10:1 and 5:1) showed a two-phase profile where the fluorescence intensity increases rapidly during initial 100 s and then reaches to a slow rise region. Kinetic profiles of the excess-base NPs were successfully fitted by an equation expressing the pre-steady-state burst kinetics[18] which is quite similar to the pre-steady-state burst kinetics of enzyme whereas single-phase kinetic behaviors for the other NPs were well suited to a typical pseudo-first-order kinetics model.[19] The single-phase NPs showed rate constants (k_{obs}) fitted in the range of 10^{-4}-10^{-5} s^{-1} (Table S1), which are comparable to the previously reported values for boronate-based H_2O_2 probes.[9,12] In sharp contrast, the highly catalyzed NPs with an initial big burst (1PI:pFS-DT=10:1) presented a greatly accelerated kinetic rate that is ten orders of magnitude higher than that of the uncatalyzed pFS-DT-alone NPs (Table S1 and Fig 3d). Such a kinetic boost with base catalysis could be a critical feature to realized a real-time imaging of H_2O_2.

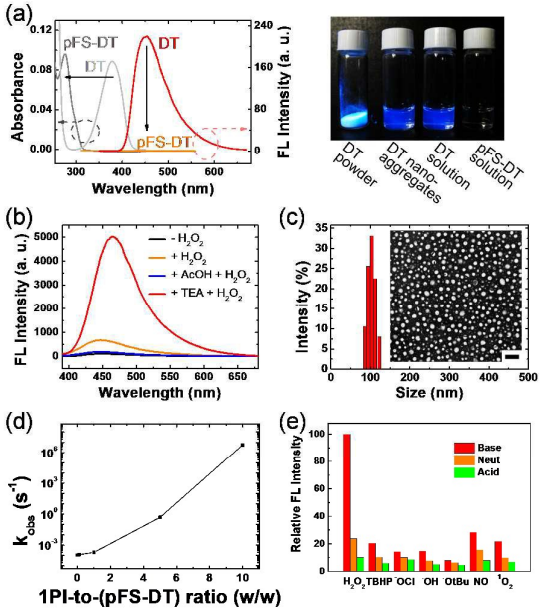

Fig 1. (a) Absorption and fluorescence spectra of DT and pFS-DT in THF and photograph showing fluorescence of samples under 365-nm illumination. (b) Fluorescence response of pFS-DT to H_2O_2 in THF in the presence or absence of a catalyst (AcOH or TEA), after a reaction time of 20 min at 25 °C. (c) Size distribution and TEM image (inset) of basic NPs (1PI:pFS-DT=10:1; scale bar: 300 nm). (d) Dependence of rate constants on the loading amounts of 1PI incorporated in NPs. (e) Fluorescence responses of basic (red, Base), neutral (orange, Neut) and acidic (green, Acid) NPs to various ROS, obtained after stirring them with 100 μM of each ROS for 60 min at room temperature.

Importantly, the base catalysis was found to provide an additional benefit of improving the selectivity of NPs toward H_2O_2 among biologically relevant ROS (Fig 1e). As reported in the literature, the pFS caging group has a marginal uncaging selectivity to H_2O_2.[13] Similar to pFs, low H_2O_2 selectivity was observed in uncatalyzed neutral NPs (pFS-DT alone) and Acidic NPs (TMBA:pFS-DT=10:1). However, the H_2O_2 selectivity was greatly enhanced in the basic NPs (1PI:pFS-DT=10:1) with a ratio of 3.5-12.6. The H_2O_2 selectivity enhancement is unambiguously attributed to the co-incorporation of base catalysis that has no catalytic effect on non-specific oxidation reactions but selectively activates perhydrolysis.

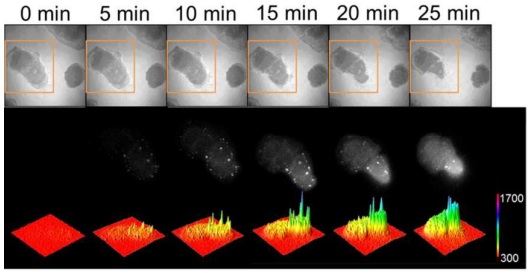

Fig 2. Temporal evolutions of bright field image (top row), fluorogenic pattern (middle) and fluorescence intensity profile (bottom) at the indicated time points after epidermal growth factor (EGF) stimulation (500 ng/mL) to A431 cells pre-treated with 0.1 mg/mL of b-NPs (1PI:pFS-DT=10:1) for 5 min. The middle and bottom rows correspond to the regions indicated with orange squares in the top row.

Taking advantage of fast kinetics and improved selectivity in cellular environment, we assessed the capability of base-catalyzed NPs (1PI:pFS-DT=10:1; referred to as b-NPs) for spatiotemporally-resolved imaging of low-level H_2O_2 generated during cellular processes. First, endogenous production of H_2O_2 in A431 cells was monitored at the very beginning of EGF stimulation (Fig 2). It is known that binding of EGF to the extracellular domain of the EGF receptor (EGFR) activates phosphatidylinositol-3-OH kinase (PI3K) and NADPH oxidase (Nox) to generate superoxide which is converted to H_2O_2 via spontaneous dismutation and then penetrates the membrane to the cytosol.[8,13,20] To see the sequence of this process in a timely manner, A431 cells were pre-treated with 0.1 mg/mL of b-NPs for 5 min, during which no fluorogenic signals were seen in the microscopic observation. Upon stimulation of the pre-treated cells with EGF (500 ng/mL), fluorescence spots with a punctate pattern evolved from localized cellular regions during initial 15 min. After the initial punctate response, fluorescence signals were gradually diffused throughout the cytosolic area with the overall intensity increased. It was observed that the signal diffusion coincides with a marked shrinkage in cell morphology (bright field images in Fig 2), which is in accordance with the EGF-modulated cell shape change reported in the literature.[20] The middle and bottom rows correspond to the regions indicated with orange squares in the top row. During the time, no notable fluorescence was detected without EGF stimulation in b-NPs treated A431 cells (Fig S6), verifying that the fluorogenic signals in Fig 2 is a response of the cell-internalized b-NPs to endogenous H_2O_2 during EGF stimulation. In the same experimental setup, a commercial ROS probe molecule, DCFH-DA, provided only a blurred and diffused response to EGF stimulation with much lower fluorescence intensity, lacking in spatiotemporal information (Fig S7). Moreover, DCFH-DA displayed its intrinsic poor characteristics of light-induced auto-oxidation before EGF stimulation and photobleaching during repetitive imaging, which was not seen with b-NPs. These distinct imaging results demonstrate that b-NPs equipped with nanoscopic base catalysis have greatly improved performances for cell imaging in terms of spatiotemporal resolution and photostability.

To confirm whether the sensing kinetics of NPs can be retained in the intracellular environment, imaging of endogenous H_2O_2 was briefly conducted with RAW264.7 macrophages that can produce high levels of H_2O_2 in response to phorbol myristate acetate (PMA).[14] After adding PMA, acidic NPs (TMBA:pFS-DT=10:1) presented a punctate pattern of fluorescence at 60 min of incubation, whereas the pattern with basic NPs (1PI:pFS-DT=10:1) could be seen at much earlier time (10 min of incubation) (Fig S5). Such distinct behaviors between acidic and basic NPs indicate that the physically assembled nanoreactor is retained stably in cells, clearly elucidating the utility of NPs as an intracellular bioprobe.

In A431 cells expressing yellow fluorescent protein (YFP)-encoded Nox1, all the fluorescently labeled Nox1 domains on the membrane overlapped with a fraction of the initial punctate spots of b-NPs (Fig S8). Considering that Nox1 is a member of Nox family (ROS-producing membrane proteins),[21] the signal co-localization between b-NPs and Nox1 concludes that b-NPs is indeed capable of visualizing an early phase of the H_2O_2 production by Nox in the EGF-induced signaling pathway with a high spatiotemporal resolution. To further confirm the origin of endogenous H_2O_2 generation, inhibition tests were conducted with chemical inhibitors (Fig S9). The fluorogenic response of b-NPs to EGF stimulation was significantly reduced by PD153035 (inhibiting EGFR kinase domain), Apocynin (inhibiting Nox), and Wortmannin (inhibiting PI3K), whereas L-NAME (inhibiting NO synthase) revealed no inhibition effect. All these reponses well reflect the mechanistic aspects of EGF-induced signaling pathway, suggesting that b-NPs with fast sensing kinetics offer a useful tool for timely visualization of cellular biological events implicated with low-level H_2O_2.

Further, the cellular impacts of b-NPs were comparatively evaluated between HeLa cells with and without sample uptake at 0.1 mg/mL (Fig. S10). It turned out that b-NPs under the given condition induce no significant alteration in both intracellular H_2O_2 and pH levels and that its cytotoxicity is negligible, indicating minimal impacts on the cellular physiology.

To explore the general utility of b-NPs in a wide range of cell processes, imaging pathology-related generation of H_2O_2 in subcellular compartments was attempted. Type II diabetes is a

disease in which a high level of nonesterified fatty acid (NEFA) leads to pancreatic β-cell dysfunction and loss (called lipotoxicity),[22] a major cause of which was found to be oxidative stress by metabolically overproduced H_2O_2 in peroxisomes.[23] As a model for such disorders, a pancreatic β-cell line (RIN-m) was stimulated with 50 μM of palmitic acid (one of NEFAs) to induce lipotoxicity. Upon uptake into the lipotoxicity-induced cells, b-NPs displayed a punctate pattern of fluorescent spots, all of which are co-localized with fluorescently labeled peroxisomes (Fig 3a), well visualizing the aforementioned pathological process occurring in subcellular compartments. With enhanced sensitivity by nanoscopic base catalysis, b-NPs was also capable of detecting extremely low levels of H_2O_2 produced during various cellular processes. Endogenous H_2O_2 in homeostatic cellular processes such as starvation[24]- and hypoxia[25]-induced autophagy was successfully imaged with b-NPs. When treated with b-NPs for 15 min, nutrient-starved cells, incubated in Earle's balanced salt solution (EBSS) for 3h, showed brighter fluorescence than cells incubated in control media (DMEM with 10 % FBS) (Fig. 3b and Fig. S11a). Similarly, the fluorescent signal of b-NPs in hypoxic (less than 1 % O_2 for 24h) HeLa cells was higher than in normoxic (20 % O_2, Ctrl.) cells (Fig. 3c and Fig. S11b). Moreover, b-NPs was capable of imaging cell proliferation involving H_2O_2 at 10^{-8} M (Fig S12)[2].

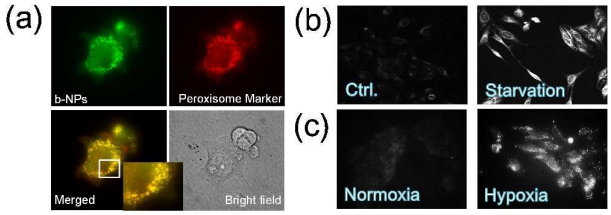

Fig 3. Fluorescence imaging of H_2O_2 produced in various cellular processes of living cells with b-NPs. (a) NEFA-induced lipotoxicity of RIN-m cells. The images show b-NPs channel, peroxisome marker channel, overlay of the two channels (merged), and bright field. The inset is a magnified image of the region marked with a white square. (b) Starvation-induced autophagy of HeLa cells (c) Hypoxia-induced autophagy of HeLa cells.

In summary, we have devised a novel concept of reactor-like nanoprobes with enzyme-like boosted sensing kinetics for fast, sensitive and selective imaging of low-level H_2O_2 generated during various cellular processes. The nanoreactor construction is based on the physical assembly of sulfonylation-quenched fluorogenic molecules and catalytic additives into an amphiphile-stabilized colloidal structure. Such a versatile probe design enabled facile control of the sensing rate to provide unprecedentedly fast sensing kinetics and improved selectivity. The base-catalyzed nanoprobes allowed for timely visualization of low-level H_2O_2 involved in various cell processes of normal and pathological physiology. All the results demonstrate that nanoscopic control of chemical sensing reaction is a rational way of tailoring the imaging performance of molecular probes, holding potential to offer a new tool for unveiling the fundamentals of cell biology.

Notes and references

1 M. D. Ferrer, A. Sureda, A. Mestre, J. A. Tur, A. Pons, *Cell. Physiol. Biochem.* 2010, **25**, 241–252; M. Valko, D. Leibfritz, J. Moncol, M. T. D. Cronin, M. Mazur, J. Telser, *Int. J. Biochem. Cell Biol.* 2007, **39**, 44–84; D. Gius, D. R. Spitz, *Antioxid. Redox Signal.* 2006, **8**, 1249–1252.
2 M. Giorgio, M. Trinei, E. Migliaccio, P. G. Pelicci, *Nat. Rev. Mol. Cell Biol.* 2007, **8**, 722–728.
3 J. R. Stone, S. Yang, *Antioxid. Redox Signal.* 2006, **8**, 243–270.
4 C. C. Benz, C. Yau, *Nat. Rev Cancer* 2008, **8**, 875–879; W. Dröge, *Physiol. Rev.* 2002, **82**, 47–95.
5 T. Finkel, *FEBS Lett.* 2000, **476**, 52–54.
6 S. Mueller, *Free Radic. Biol. Med.* 2000, **29**, 410–415.
7 K. J. Davies, A. T. Quintanilha, G. A. Brooks, L. Packer, *Biochem. Biophys. Res. Commun.* 1982, **107**, 1198–1205; S. G. Wannamethee, A. G. Shaper, M. Walker, *Lancet* 1998, **351**, 1603–1608.
8 B.C Dickinson, C. J. Chang, *Nat. Chem. Biol.* 2011, **7**, 504–511.
9 N. M. Mishina, P. A. Tyurin-Kuzmin, K. N. Markvicheva, A. V. Vorotnikov, V. A. Tkachuk, V. Laketa, C. Schultz, S. Lukyanov, V. V. Belousov, *Antioxid. Redox Signal.* 2011, **14**, 1–7.
10 Y. V Mukhin, M. N. Garnovskaya, G. Collinsworth, J. S. Grewal, D. Pendergrass, T. Nagai, S. Pinckney, E. L. Greene, J. R. Raymond, *Biochem. J.* 2000, **347**, 61–67; A. S. Keston, R. Brandt, *Anal. Biochem.* 1965, **11**, 1–5; H. Wang, J. Joseph, *Free Radic. Biol. Med.* 1999, **27**, 612–616.
11 E. W. Miller, A. E. Albers, A. Pralle, E. Y. Isacoff, C. J. Chang, *J. Am. Chem. Soc.* 2005, **127**, 16652–16659; B. C. Dickinson, C. J. Chang, *J. Am. Chem. Soc.* 2008, **130**, 9638–9639.
12 E. W. Miller, O. Tulyathan, E. Y. Isacoff, C. J. Chang, *Nat. Chem. Biol.* 2007, **3**, 263–267.
13 B. C. Dickinson, C. Huynh, C. J. Chang, *J. Am. Chem. Soc.* 2010, **132**, 5906–5915.
14 H. Maeda, Y. Fukuyasu, S. Yoshida, M. Fukuda, K. Saeki, H. Matsuno, Y. Yamauchi, K. Yoshida, K. Hirata, K. Miyamoto, *Angew. Chem. Int. Ed.* 2004, **43**, 2389–2391.
15 K. Xu, B. Tang, H. Huang, G. Yang, Z. Chen, P. Li, L. An, *Chem. Commun.* 2005, 5974–5976.
16 D. Casanova, C. Bouzigues, T.-L. Nguyên, R. O. Ramodiharilafy, L. Bouzhir-Sima, T. Gacoin, J.-P. Boilot, P.-L. Tharaux, A. Alexandrou, *Nat. Nanotechnol.* 2009, **4**, 581–585; H. Jin, D. A. Heller, M. Kalbacova, J.-H. Kim, J. Zhang, A. A. Boghossian, N. Maheshri, M. S. Strano, *Nat. Nanotechnol.* 2010, **5**, 302–309.
17 S. L. Newmyer, P. R. O. De Montellano, *J. Biol. Chem.* 1995, **270**, 19430–19438; M. I. Savenkova, S. L. Newmyer, P. R. Ortiz de Montellano, *J. Biol. Chem.* 1996, **271**, 24598–24603; S. S. Dong, K. J. Du, Y. You, F. Liu, G. B. Wen, Y. W. Lin, *J. Electroanal. Chem.* 2013, **708**, 1–6.
18 A. Roa, M. L. Goble, J. L. García, C. Acebal, R. Virden, *Biochem. J.* 1996, **316**, 409–412.
19 D. J. O'Shannessy, D. J. Winzor, *Anal. Biochem.* 1996, **236**, 275–283.
20 C. E. Paulsen, T. H. Truong, F. J. Garcia, A. Homann, V. Gupta, S. E. Leonard, K. S. Carroll, *Nat. Chem. Biol.* 2012, **8**, 57–64.
21 J. D. Lambeth, *Nat. Rev. Immunol.* 2004, **4**, 181–189.
22 E. S. Gordon, *Am. J. Clin. Nutr.* 1960, **8**, 740–747; V. Poitout, R. P. Robertson, *Endocrinology* 2002, **143**, 339–342.
23 M. Elsner, W. Gehrmann, S. Lenzen, *Diabetes* 2011, **60**, 200–208.
24 R. Scherz-Shouval, E. Shvets, E. Fass, H. Shorer, L. Gil, Z. Elazar, *EMBO J.* 2007, **26**, 1749-1760.
25 J. J. Zulueta, F. S. Yu, I. A. Hertig, V. J. Thannickal, P. M. Hassoun, *Am. J. Respir. Cell Mol. Biol.* 1995, **12**, 41-49.